Chemical Physics Letters 459 (2008) 188–193

Contents lists available at ScienceDirect

Chemical Physics Letters

journal homepage: www.elsevier.com/locate/cplett

Solid-state single-scan 2D NMR under magic-angle-spinning

Maayan Gal [a], Claudiu Melian [b], Dan E. Demco [b,c], Bernhard Blümich [b], Lucio Frydman [a,*]

[a] Department of Chemical Physics, Weizmann Institute of Science, 76100 Rehovot, Israel
[b] Institute for Technical and Macromolecular Chemistry, RWTH Aachen D-52074, Germany
[c] DWI an der RWTH Aachen e.V., Pauwelsstrasse. 8, D-52056 Aachen, Germany

ARTICLE INFO

Article history:
Received 16 January 2008
In final form 15 May 2008
Available online 21 May 2008

ABSTRACT

Few analytical techniques rival the capabilities of two-dimensional nuclear magnetic resonance. A scheme enabling 2D NMR acquisitions within a single-scan has been recently demonstrated, based on combined field gradient and radiofrequency manipulations. Distortions were observed upon implementing such 'ultrafast' experiments on solids undergoing magic-angle-spinning, presumably due to interferences arising between the periodic time-dependencies involved in the mechanical and in the spin manipulations. Experimental and numerical setups were designed to investigate these effects, and to find conditions that minimize them. When devoid of these non-idealities, quality 2D NMR spectra could be retrieved from spinning polymers within a single-scan.

1. Introduction

Two-dimensional (2D) spectroscopy constitutes one of the cornerstones supporting the chemical, biological, and clinical applications of nuclear magnetic resonance (NMR) [1,2]. 2D NMR is also a basic tool in Material Sciences, having become a standard for screening organic and inorganic substrates in several settings [3–6]. 2D magic-angle-spinning (MAS) NMR methods in particular provide a straightforward route to the elucidation of synthetic polymer structures, allowing through their superior resolution characteristics to establish the nature of sites and the characterization of relative arrangements and dynamics over a wide range of space- and time-scales. There may, however, be a drawback associated with relying on experiments with increasing dimensionalities, stemming from the potentially longer times needed for collecting these data. This problem is well known in many important realms of NMR, including in high-throughput screening modes aiming at the systematic investigation of large numbers of solid samples such as those made available by combinatorial approaches employing different processing parameters [7,8].

Driven in part by this constraint recent years have witnessed the emergence of alternatives capable of speeding up the acquisition of 2D NMR data [9,10], including so-called 'ultrafast' approaches capable of completing arbitrary nD NMR experiments within a single-scan [11–13]. Such proposal endows different spin-packets within a resonance that has been subject to an inhomogeneous broadening, with the equivalent of different increments in their indirect-domain time evolutions. Although when dealing with solids it is conceivable to rely on the anisotropic character of spin interactions to impart such inhomogeneous broadening [14], the most straightforward way of doing this is by applying suitably-refocused linear field gradients $\vec{G} = G_0\hat{g}$, imposing different frequencies on different positions within the sample. A train of frequency-incremented or frequency-chirped radiofrequency (RF) pulses can then be used to excite, refocus or store the spins' evolution progressively as a function of their spatial positions. This will impose a spatial winding on the spins' magnetization M that parallels the gradients $\hat{g}$ geometry, whose magnitude is controlled by the indirect-domain $I(\Omega_1)$ spectrum one is attempting to measure according to

$$M(r) \approx \sum_{\Omega_1} I(\Omega_1)\exp[\mathrm{i}C\Omega_1 r], \tag{1}$$

where Ω_1 represents the spins' chemical shift and C is a parameter under experimental control. Unlike conventional time-domain procedures, this imprinting can be implemented over the full desired range $0 \leqslant t_1 \leqslant t_1^{\max}$ of evolution times within a single-scan. Such spatially encoded information will be coherently preserved throughout the sequence's mixing process, and can be subsequently read-out by a G_a acquisition gradient possessing the same geometry as its encoding counterpart. When such gradient is applied, spins become subject to the action of an additional acquisition wavenumber $k(t) = \gamma_a \int_t G_a(t')\mathrm{d}t'$, leading to signals that when integrated over the sample's length L

$$\begin{aligned} S[k(t)] &\approx \sum_{\Omega_1} I(\Omega_1) \int_L \exp[\mathrm{i}C\Omega_1 r]\exp[\mathrm{i}k(t)r]\mathrm{d}r \\ &\approx \sum_{\Omega_1} I(\Omega_1)\delta[C\Omega_1 + k] \end{aligned} \tag{2}$$

read-out the indirect-domain frequency spectrum $I(\Omega_1)$ as echoes along the k/v_1 frequency axis –no Fourier transformations involved.

* Corresponding author. Fax: +972 8 9344123.
E-mail address: Lucio.Frydman@weizmann.ac.il (L. Frydman).

0009-2614/$ - see front matter © 2008 Elsevier B.V. All rights reserved.
doi:10.1016/j.cplett.2008.05.045

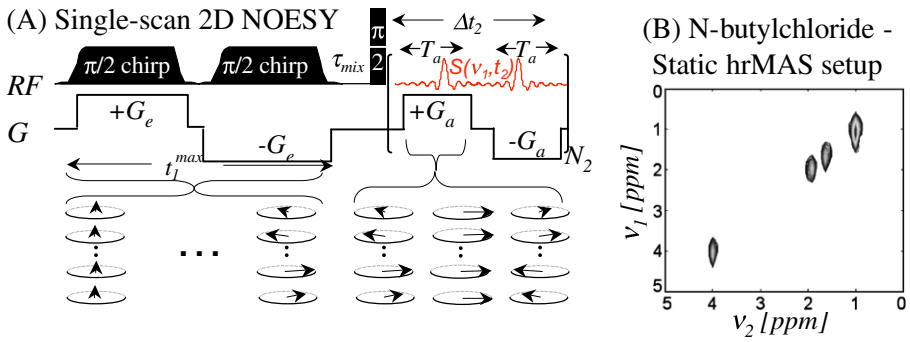

Fig. 1. (A) Single-scan 2D NOESY-type sequence assayed throughout this study. The first two chirped RF pulses carry a spatial encoding of the indirect-domain interactions, while the oscillating $\pm G_a$ gradients do a repetitive read-out of their $I(\Omega_1)$ spectra as a function of time t_2. (B) Single-scan 2D NMR spectrum acquired upon executing the sequence in (A) on a liquid *n*-butylchloride sample, using a gradient-equipped MAS NMR probe (fixed gradient coil) under non-spinning conditions. Data were recorded at 11.7 T with G_e = 14 G/cm, chirp pulses sweeping 100 kHz over 10 ms, τ_{mix} = 100 ms, G_a = 40 G/cm, N_2 = 64, T_a = 400 μs (gradient pulses of 350 μs, gradient-switching times of 50 μs, and a constant sampling time of 2 μs). A 400 μs purging gradient *P* of 14 G/cm was applied just prior to the beginning of the data digitization. The acquired data points were separated for processing into $+G_a$ and $-G_a$ contributions; the plot illustrated here resulted from subjecting one of these sets to a suitable shearing, zero-filling to 128 × 256 (k, t_2)-points, Fourier transformation against t_2, and magnitude mode calculation. The total experimental time was 0.3 s.

Moreover the times T_a over which G_a needs to be applied are fairly short; suffice it to make $k_{max} = \gamma_a G_a T_a$ equal to the spectral window SW_1 to be explored scaled by the $C \approx t_1^{max}/L$ coefficient, leading to $T_a \approx t_1^{max} \frac{SW_1}{\gamma_a G_a L}$ of a few 100's of μs. This interval is much shorter than common T_2 decays, implying that the G_a-driven read-out process can be done and undone numerous times over the course of a single acquisition. Such repeated oscillations will generate a train of k/Ω_1-echoes, modulated as a function of the direct-domain evolution frequencies Ω_2 acting during the course of t_2

$$S[k(t_2), t_2] \approx \sum_{\Omega_2} \sum_{\Omega_1} I(\Omega_1, \Omega_2)\delta[C\Omega_1 + k] \exp[i\Omega_2 t_2] \quad (3)$$

Fourier transformation of the resulting $S[k(t_2), t_2]$ array against t_2 will thereby provide the 2D $I(\Omega_1, \Omega_2)$ NMR spectrum being sought – still, while confined within a single-scan. Both the overall principles as well as practical examples of this novel 2D NMR approach are presented for completion for an amplitude-modulated exchange-type sequence in Fig. 1 [15], implemented using a bipolar encoding gradient acting in synchrony with two identical π/2 RF sweeps [16] on a high-resolution gradient-equipped MAS NMR probe. While these principles were demonstrated for a range of organic and biomolecular samples in the liquid phase, they have not to our knowledge been hitherto reported on samples undergoing MAS. Analyzing the novel aspects that may arise in such spinning-case scenario constitutes the main aim of this Letter.

2. Experimental methods

Single-scan 2D ^{1}H NMR experiments were acquired on liquid and rubber samples, using two complementary setups. One of these involved a commercial 11.7 T NMR spectrometer equipped with a gradient-enhanced 4 mm MAS NMR probe, providing a fixed gradient orientation along the rotor's axis with strengths of up to 50 G/cm and spinning rates up to 15 kHz. The other involved a 7.1 T microimaging scanner, equipped with a multi-axis (G_x, G_y, G_z) accessory capable of delivering up to 100 G/cm gradients along three orthogonal directions. This allowed us to orient the secular components of the magnetic field gradient $\vec{G} = \vec{\nabla} B_z = G_0 \hat{g}$, at arbitrary orientations *vs.* the axis of sample rotation. A narrow-bore probehead equipped with a 2.5 mm spinner capable of executing MAS at rates up to 35 kHz was then stripped away from its normal casing, shielded with aluminum foil to reduce eddy currents while minimizing RF interferences, and installed within this gradient set. An important component of the tests carried out using this setup required finding the MAS rotor orientation within the $\vec{\nabla} B_z$ gradient frame. A reliable way for doing so was found by arraying a simple gradient-echo experiment with fixed timing and gradient strength $G_0 = \sqrt{G_x^2 + G_y^2 + G_z^2}$ over a range of $G_x/G_y/G_z$ combinations, corresponding to a full exploration of the $\hat{g}$ orientation over the solid sphere (Fig. 2A). The resulting images consist of a series of 1D profiles whose intensities peak over a characteristic, well-defined band of values (Fig. 2B) corresponding to $\hat{g}$ orientations that are normal to the rotor's long cylindrical axis. A spherical representation of these values defines then a single central azimuth point (θ_{rot}, φ_{rot}), orienting the MAS spinning axis within the laboratory frame defined by the orthogonal gradient set (Fig. 2C). A more practical yet essentially equivalent way to retrieve this desired orientation consists of looking first for the normal to the rotor axis within the (G_x,G_y) plane by finding the sharpest profile arising for a fixed G_0 value while keeping $G_z = 0$; with φ_{rot}'s value thus defined, the sharpest profile obtained as a function of different G_z components enables an unambiguous determination of θ_{rot}. The rotor axis could thereby be defined using two rapid 1D searches (instead of a full 2D one) prior to each measurement on either liquids and solids; with this at hand it was feasible to explore the effects that misaligning $\hat{g}$ and the axis of MAS had on the acquisition of ultrafast 2D NMR data on rotating samples.

3. Results and discussion

Implementing ultrafast 2D NMR schemes under MAS conditions should not present a significant challenge, provided that the gradient's $\hat{g}$ orientation is aligned along the orientation of the rotor axis. Sample spinning effects can then be decoupled from gradient manipulations [17–19] rendering an experiment that, at least from the standpoint of the ultrafast encoding and decoding processes, approaches static-like conditions. Based on such assumption the gradient-equipped MAS probehead used to record the static liquid spectrum in Fig. 1, was employed to execute a similar 2D NOESY-type acquisition under sample spinning conditions. Fig. 3A illustrates results obtained upon employing this setup to carry out a MAS NMR experiment on a natural rubber sample. Even if repeated over a wide variety of spinning rates and/or gradient strengths, the resulting single-scan 2D experiments yielded few of the easily recognizable spectral features arising when executing 2D cross-relaxation NMR on the same platform with a conventional time-domain protocol (Fig. 3B). The reasons underlying this discrepancy between expectation and reality could be many, yet the good results observed under non-spinning conditions (Fig. 1) suggest discarding

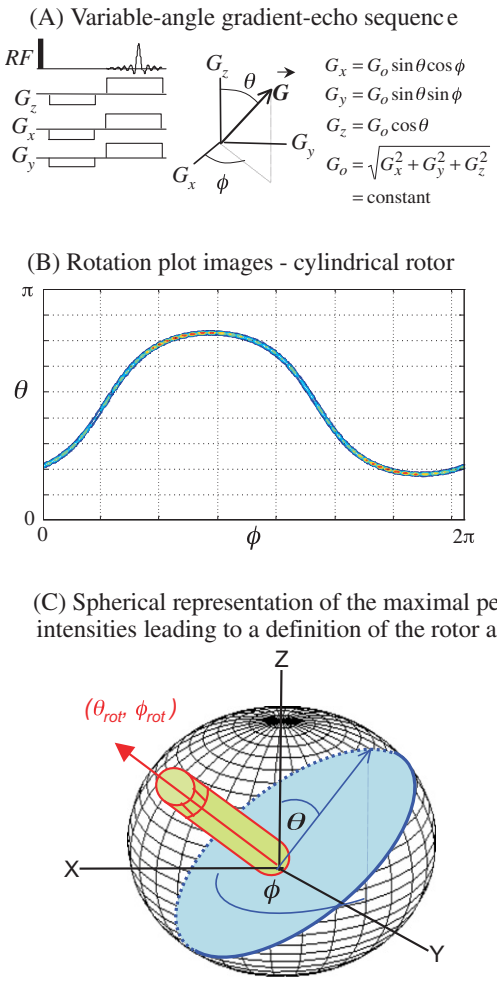

Fig. 2. Strategy employed to find the exact (θ_{rot}, φ_{rot}) orientation of the MAS rotor, within a laboratory frame defined by the three orthogonal components of a magnetic field gradient set. (A) A gradient-echo pulse sequence is arrayed, given by a constant overall G_0 gradient strength but varying (G_x, G_y, G_z) components defining different (θ, φ) angles within a laboratory frame. Changing the resulting polar and azimuthal angles yields an array of 1D sample profiles, whose area is constant but width is minimal when the gradient's orientation $\hat{g}$ is normal to the rotor axis. This is illustrated in (B), which shows the ensuing maximum-strength contour plots for an experimental set collected on a 7.1 T microimaging scanner. (C) Arraying the resulting (θ, φ) maximal values in a spherical representation yields a well-defined azimuth, providing an exact orientation of the rotor within the laboratory frame.

those related to poor performances of the RF or to typical gradient setup faults such as eddy currents or slow rise/fall times. This in turn points towards complications associated to the act of mechanical spinning itself, including potential interferences between the various time-dependencies that are present in this experiment.

In order to obtain a better idea on how such factors could interfere with a typical ultrafast 2D acquisition, numerical simulations were carried out capable of solving relaxation-free time-dependent Bloch equations

$$\begin{aligned}
\frac{\partial}{\partial t}M_x(t,\vec{r}) &= -[\Omega_1 + \gamma G_0(t)\hat{g}\cdot\vec{r}(t)]M_y(t,\vec{r}) + \gamma B_1(t)\sin[\varphi_{RF}(t)]M_z(t,\vec{r}) \\
\frac{\partial}{\partial t}M_y(t,\vec{r}) &= +[\Omega_1 + \gamma G_0 t)\hat{g}\cdot\vec{r}(t)]M_x(t,\vec{r}) - \gamma B_1(t)\cos[\varphi_{RF}(t)]M_z(t,\vec{r}) \\
\frac{\partial}{\partial t}M_z(t,\vec{r}) &= -\gamma B_1(t)\sin[\varphi_{RF}(t)]M_x(t,\vec{r}) + \gamma B_1(t)\cos[\varphi_{RF}(t)]M_y(t,\vec{r})
\end{aligned} \tag{4}$$

Notice that within this setting not only the spins' positions $\vec{r}$ but also the gradient's amplitude G_0 as well as the RF's amplitudes γB_1 and phases (i.e., frequencies) ϕ_{RF} are allowed to be time-dependent, so as to accommodate the potential effects that sample rotation, gradient oscillations and sweeping offsets could have in the single-scan 2D MAS NMR acquisition. A time propagation of these equations and integration of their resulting transverse complex magnetizations over all possible positions throughout a cylindrical rotor volume

$$S(t) \approx \int_V [M_x(t,\vec{r}) + iM_y(t,\vec{r})]d\vec{r} \tag{5}$$

should then mimic the expected experimental signal behavior. This is in fact the same approach as normally used in the simulation of conventional liquid-state ultrafast NMR experiments, except for the fact that in those cases $\hat{g} \equiv \hat{z}$ and $\vec{r}(t)$ simply needs to consider a set of time-independent z coordinates through a sample length L.

With this numerical tool available and with the possibility to experimentally adjust the relative orientation between $\hat{g}$ and the axis of MAS rotation, we set out to explore what new effects could then arise during the implementation of ultrafast 2D acquisitions. Both experiments and simulations confirmed that an exact alignment of $\hat{g}$ along the axis of sample spinning and rapid enough spinning rates, do indeed enable the acquisition of ultrafast 2D MAS NMR data showing usual features. Fig. 4 illustrates this with a series of exchange-type 2D contour plots, collected on a sample of natural rubber using a sequence analogous to that employed in Fig. 3 but with the field gradient accurately oriented along the (θ_{rot}, φ_{rot}) direction as described in Experimental Methods. Although the data quality that can be inferred from these results is somewhat lower than that in conventional 2D cross-relaxation experiments, they certainly show several of the features that could be expected from this kind of experiments. Fig. 4A for instance exemplifies how, only at high enough spinning rates, will the 2D traces display sharp ^{1}H centerbands devoid from spinning sidebands – which will

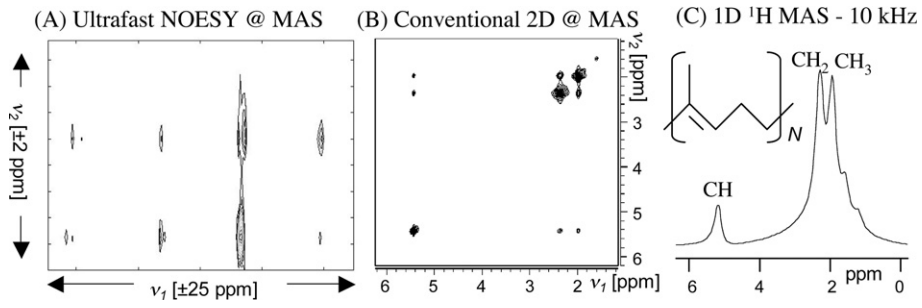

Fig. 3. (A) Single-scan ^{1}H 2D cross-relaxation NMR spectra of natural rubber recorded on the same equipment as used to collect the data in Fig. 1, but this time subject to 10 kHz MAS rates. Experimental conditions were akin to those employed in that earlier run, except for the spinning and for a shorter mixing (τ_{mix} = 5 ms). (B) 2D NMR spectrum collected under similar spinning and timing conditions on the same rubber sample, using a conventional acquisition mode. Shown for completion in (C) is the analyzed polymer and its single-pulse high-resolution ^{1}H NMR spectrum at 10 kHz MAS.

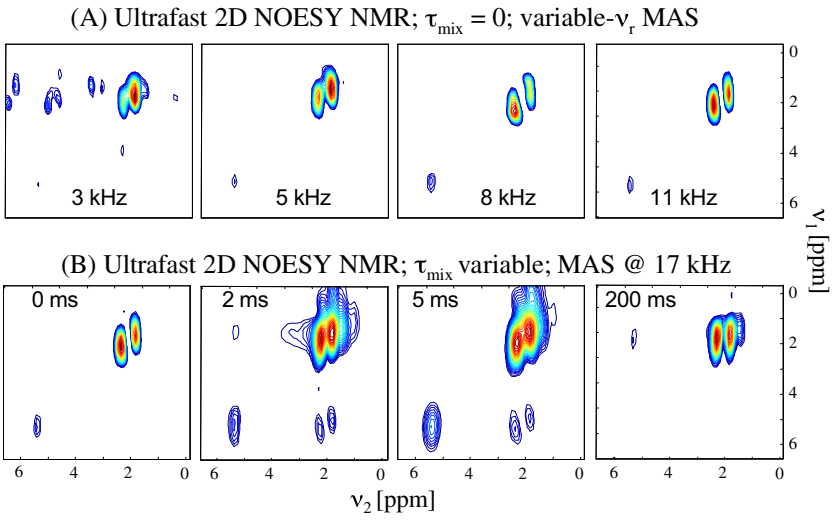

Fig. 4. Series of single-scan 2D ^{1}H exchange NMR spectra collected on natural rubber at different spinning rates and mixing times, using a 7.1 T microimaging setup where the effective gradient orientation has been adjusted to coincide with (θ_{rot}, φ_{rot}). Acquisitions parameters: G_e = 33 G/cm, RF pulses sweeping over 130 kHz during $t_1^{max}/2 = 7$ms, G_a = 30 G/cm, T_a = 240 μs, N_2 = 32 and zero-filling of the final data to a full 128 × 64 matrix size.

otherwise fold over due to the large filter bandwidths with which the single-scan 2D NMR experiment needs to operate. Fig. 4B in turn shows the build-up of cross-peaks and subsequent fall of both inter- and intra-site resonances, when viewed as a function of the cross-relaxation mixing time. Also evident is an asymmetry in the intensities of off-diagonal cross-peaks, which though expected is more marked than in the conventional Fig. 3B counterpart.

Although both simulations and experiments suggest that reliable single-scan 2D NOESY MAS data can be obtained under optimized circumstances, both approaches point to towards significant spectral non-idealities when small misalignments Δ between the gradient's and the MAS axes orientations arise. Indeed under such conditions, the gradient-derived phase φ_G accrued by spins positioned at spherical coordinates $\vec{r} = (\rho, \beta, \alpha)$ within the rotating sample, will reflect two contributions of differing nature (Fig. 5A): a rotationally-invariant one arising from the projection of $\hat{g}$ onto the axis of rotation, and a time-dependent one associated to $\hat{g}$'s transverse component:

$$\begin{aligned}\phi_G(\alpha,\beta,\rho,t) &= \gamma\int_0^t \mathrm{d}t'\vec{G}(t')\cdot\vec{r}(t') \\ &= \gamma\rho\int_0^t \mathrm{d}t' G_0(t')[gr_{//}+gr_{\perp}(t')] \\ &= \gamma\rho\int_0^t \mathrm{d}t' G_0(t')[\cos\Delta\cos\beta+\sin\Delta\sin\beta\cos(\alpha \\ &\quad +2\pi\nu_{rot}t')], \end{aligned} \tag{6}$$

where ν_{rot} denotes the MAS spinning rate. Because of their spectroscopic nature ultrafast NMR experiments design $G_0(t)$ so as to average out the net effects of the gradients, oscillating G_0 to make $\phi_G(t_1^{max}) \approx 0$ at the conclusion of the indirect-domain evolution and $\phi_G(t_2) \approx 0$ within each sampling direct-domain dwell time. 2D MAS NMR experiments operating under the ideal $\Delta = 0$ condition meet these demands, regardless of the spin's position. Upon misaligning the gradient away from the MAS axis, however, a new $gr_{\perp}(t)$ time-dependence arises, capable of interfering with this original balancing out of the gradients. Each (ρ,β,α) position will then experience its own set of non-zero φ_G phases, leading to a rapid irreversible decay when considering signals $S(t) = \int_V I(\Omega_1,\Omega_2)\exp[i\phi_G(t,\vec{r})]\mathrm{d}\vec{r}$ arising from a full sample volume.

It follows from these arguments that two main processes may be susceptible to the onset of gradient/MAS interferences. One of these will make $\varphi_G \neq 0$ at the completion of the indirect-domain spatial encoding; the other will do the same during the progress of the t_2 signal acquisition. If relying on bipolar $\pm G_e$ modulations of the kind employed in Figs. 1 or 3 [16] the first of these effects will be minor, and experimental efforts to detect them were in fact inconclusive. By contrast, both experiments and numerical simulations point towards the presence of potentially strong φ_G interferences arising during the course of t_2 upon making $\Delta \neq 0$. The strength of these effects can be understood from the very similar time-scales involved in the MAS, given by a rotor period T_{rot} in the order of 100 μs, and by $G_0(t)$ oscillations given by periods Δt_2 of similar duration. Considering for concreteness a square-wave decoding gradient oscillation of basic frequency $(2T_a)^{-1}$

$$G_0(t) = G_a\cdot\mathrm{sgn}\left[\sin(2\pi\frac{t}{2T_a})\right] = \frac{4G_a}{\pi}\sum_{n=1,3,5\ldots}^{\infty}\frac{\sin(n\pi\frac{t}{T_a})}{n} \tag{7}$$

it follows from Eq. (6) that destructive interferences are expected whenever the spinning rate $\nu_{rot} \approx (\frac{n}{2T_a})_{n=1,3,5\ldots}$. Fig. 5B evidences this effect, with calculations showing the normalized integrated intensity expected from the $S(t)$ signal for a realistic $2T_a$ = 200 μs dwell time, as a function of increasing rates of sample rotation and for a range of Δ misalignments. Notice the periodicity of the signal attenuation, as well as the decreasing (even if still strong) nature of this effect as the order n of the interfering harmonic increases or as the Δ misalignment decreases. It follows from this kind of analyses that even small (≤3°) misalignments can bring about unacceptable signal losses and concomitant peak distortions when operating near the $\nu_{rot} \approx (\frac{n}{2T_a})_{n=1,3,5\ldots}$ resonant conditions; while Δ values exceeding ≈20° bring about spectral distortions over a much wider, continuous range of speeds extending all the way up to the maximal spinning rates currently used in this kind of experiments. In a second manifestation of these interferences, Fig. 5C illustrates experimental time-domain signals collected for fixed Δ = 30° and ν_{rot} = 5 kHz values as a function of changing T_a gradient oscillation times, for both a liquid and a solid sample. Owing to its longer T_2 transverse relaxation decay the former sample evidences more clearly the above-mentioned interference; in both instances, however, the fast decay trend for the $T_a \approx (\frac{n}{2\nu_{rot}})_{n=1,3,..}$ condition is apparent.

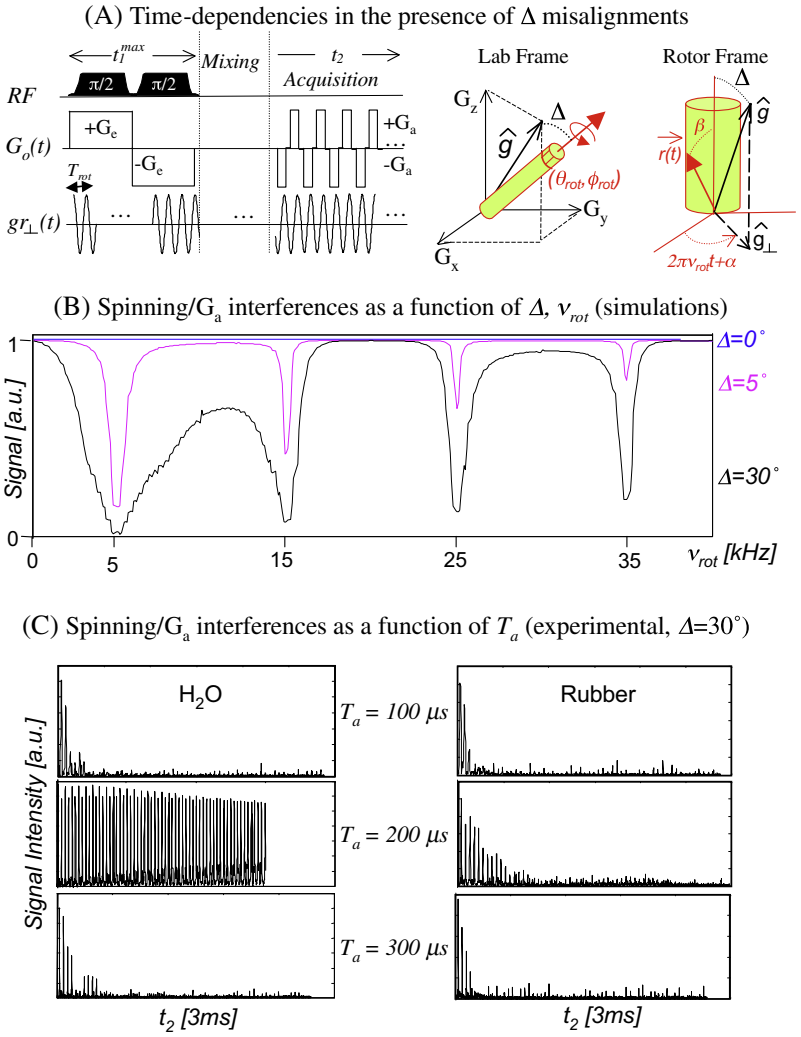

Fig. 5. (A) New time-dependencies and different angle definitions arising upon having a misalignment Δ between the field gradient employed to implement spatial encoding/decoding, and the axis of MAS. (B) Simulated data showing gradient-rotor interference effects during t_2 for a set of fixed decoding parameters (T_a = 100 μs, G_a = 20 G/cm, N_2 = 16) calculated as a function of the MAS spinning rate ν_{rot} for different Δ's. Plotted in the graphs is the overall integral of the signal's magnitude $\int_{t_2} |S(t)|dt$, yielding a description of the periodic destructive interference effects as a function of spinning frequency. (C) Experimental examples of the t_2 interference effects on water (left) and rubber (right) samples when an off-angle of 30° is inserted between the gradient- and the rotor-axes during acquisition. Spinning speed was now kept constant at 5 kHz, and the indicated T_a durations were changed. The sequence used is as in Fig. 1 with G_e = 30 G/cm, G_a = 33 G/cm, RF chirp duration = 3 ms, N_2 = 64.

4. Conclusions

The combination of gradient-based single-scan 2D NMR procedures with MAS could yield significant benefits, and is a simple procedure provided that the spectrometer delivers the required performance. As shown by this study such requirements can be met by existing pulse sequences, if commercial MAS and microimaging setups are combined and their relevant axes are precisely co-aligned. Given these facts, one could conceive furthering the kind of work hereby presented in two complementary research directions. One involves a spectroscopic route, whereby different alternatives are explored so as to alleviate the stringent demands imposed by the MAS on the gradient's alignment. In this respect it is likely that constant-gradient t_2 decoding approaches of the kind that have been recently demonstrated [20], could be more immune to Δ gradient deviations than their oscillating-gradient counterparts. Another, more applied direction, concerns exploiting the kind of measurements that were successfully illustrated in this study, to explore by NMR solid systems that are not amenable to lengthy conventional 2D acquisitions. Given the signal-to-noise limitations of single-scan 2D experiments we envision that such studies will mostly entail ^{1}H observations; given MAS limitations to deliver high-resolution in such instances, studies on soft- or semi-solids like the one analyzed in this work appear as most likely targets. Even under such constraint several applications can be conceived, involving for example studies on unstable samples, dynamic experiments monitoring the return of chemical systems back to equilibrium, or measurements on hyperpolarized samples. We trust to report on some of these avenues in the near future.

Acknowledgments

We are grateful to Koby Zibzener for valuable assistance with the MAS setup, and to Dr. Rangeet Bhattacharyya for programming discussions. This work was supported by the German–Israel Fund for Research (GIF 782/2003), and made possible by the generosity of the Perlman Family Foundation.

References

[1] R.R. Ernst, G. Bodenhausen, A. Wokaun, Principles of Nuclear Magnetic Resonance in One and Two Dimensions, Clarendon Press, Oxford, 1987.

[2] D.M. Grant, R.K. Harris (Eds.), Encyclopedia of NMR, J. Wiley & Sons, Chichester, 1996.
[3] B. Blümich, NMR Imaging of Materials, Clarendon Press, Oxford, 2000.
[4] V.J. McBriety, K.J. Packer, Nuclear Magnetic Resonance in Solid Polymers, Cambridge University Press, Cambridge, 1992.
[5] K. Schmidt-Rohr, H.W. Spiess, Multidimensional Solid-State NMR and Polymers, Academic Press, London, 1994.
[6] J.J. Fitzgerald, Ed., Solid-state NMR Spectroscopy of Inorganic Materials, ACS Symp. Series 717, 1999.
[7] P.G. Schultz, X.-D. Xiang, Curr. Opin. Solid State Mater. Sci. 3 (1998) 153.
[8] M.J. Shapiro, J.R. Wareing, Curr. Opin. Chem. Biol. 2 (1998) 372.
[9] E. Kupce, R. Freeman, J. Biomol. NMR 27 (2003) 101.
[10] H.S. Atreya, T. Szyperski, Methods Enzymol. 394 (2005) 78.
[11] L. Frydman, T. Scherf, A. Lupulescu, Proc. Natl. Acad. Sci. USA 99 (2002) 15858.
[12] L. Frydman, T. Scherf, A. Lupulescu, J. Am. Chem. Soc. 125 (2003) 9204.
[13] L. Frydman, Compts. Rends. Chim. 9 (2006) 336.
[14] R. Bhattacharyya, L. Frydman, J. Am. Chem. Soc. 128 (2006) 16014.
[15] J. Jeener, B.H. Meier, P. Bachmann, R.R. Ernst, J. Chem. Phys. 71 (1979) 4546.
[16] Y. Shrot, B. Shapira, L. Frydman, J. Magn. Reson. 171 (2004) 162.
[17] D.G. Cory, W.S. Veeman, J. Magn. Reson. 82 (1989) 374.
[18] W.E. Maas, F.H. Laukien, D.G. Cory, J. Am. Chem. Soc. 118 (1996) 13085.
[19] D.E. Demco, B. Blümich, Concepts Magn. Reson. 12 (2000) 269.
[20] Y. Shrot, L. Frydman, J. Chem. Phys. 125 (2006) 204507.